Boundary-Layer and Wake Measurements on a Swept, Circulation-Control Wing

Frank W. Spaid*
McDonnell Douglas Corporation, St. Louis, Missouri 63166
and
Earl R. Keener†
NASA Ames Research Center, Moffet Field, California 94035

Wind-tunnel measurements of boundary-layer and wake velocity profiles are presented for a swept, circulation-control wing. The model is a semispan, rectangular wing with a constant cross section mounted on the tunnel sidewall at a sweep angle of 45 deg. A circulation-control slot is located ahead of the trailing edge on the upper surface. Flow surveys were obtained at midsemispan at freestream Mach numbers of 0.425 and 0.70. Boundary-layer profiles measured on the forward portions of the wing are approximately streamwise and two dimensional. The flow in the vicinity of the jet exit and in the near wake is highly three dimensional. The jet flow near the slot on the Coanda surface is directed normal to the slot. Near-wake surveys show large outboard flows at the center of the wake. The variation in the lower-surface separation location with blowing rate was determined from boundary-layer measurements at Mach 0.425. In addition to providing an experimental description of a complex, three-dimensional flowfield, these data should serve as test cases for computational fluid dynamics methods.

Nomenclature

C_f = local skin-friction coefficient, τ_w/q_e
C_p = pressure coefficient, $(p-p_\infty)/q_\infty$
C_μ = jet momentum coefficient, $m_j V_j/q_\infty S$
c = streamwise wing chord
c_l = section lift coefficient
M = Mach number
m_j = jet mass-flow rate
p = pressure
q = dynamic pressure, $(1/2)\rho u^2$
Re_c = Reynolds number based on chord
S = wing area, defined as the product of the slot length and the wing chord measured normal to the section generators
u = velocity magnitude
u_τ = shear velocity, $\sqrt{\tau_w/\rho_w}$
V_j = computed jet velocity assuming isentropic expansion from jet stagnation pressure to p_∞
x = coordinate measured parallel to freestream direction
z = coordinate normal to wing plane
α = wing angle of attack, angle between u_∞ and a projection of the model chord line measured in a plane parallel to the tunnel sidewall
β = yaw-plane flow direction angle, positive outboard
ν = kinematic viscosity
ρ = density
τ_w = wall shear stress

Subscripts

e = conditions at edge of boundary layer
j = jet parameter
∞ = freestream conditions

Received Feb. 3, 1990; revision received Dec. 14, 1990; accepted for publication Dec. 31, 1990.

*Chief Scientist, McDonnell Douglas Research Laboratories, Mail Code 222/110/1111041, P. O. Box 516. Associate Fellow AIAA.

†Research Scientist, Fluid Dynamics Research Branch, MS 230-2; currently Research Scientist, Eloret Institute, 3788 Fabian Way, Palo Alto, CA 94303. Associate Fellow AIAA.

Introduction

A TYPE of circulation control that is currently under investigation is tangential blowing from a slot located ahead of a rounded trailing edge. The tendency of the flow to adhere to the trailing edge surface is known as the Coanda effect. The deflected flow can increase the lift of a wing section to several times that obtained by the conventional method of increasing the angle of attack. Wood and Nielsen[1] present a summary of circulation-control research.

A cooperative investigation of the boundary layer and wake of a swept, circulation-control wing was conducted by NASA Ames Research Center and McDonnell Douglas Research Laboratories in the NASA Ames 6 × 6-Ft Transonic/Supersonic Wind Tunnel. The test was conducted in support of the NASA X-Wing stopped-rotor research vehicle, which is designed to cruise at high speed with the rotor stopped in the X-wing configuration.[1]

This paper presents results of boundary-layer and wake measurements at Mach numbers of 0.425 and 0.70 at a 45-deg sweep angle. More detailed descriptions of this investigation are presented in Refs. 2 and 3. Pressure measurements and oil-flow photographs are presented by Keener et al.[4] The primary value of this material is to provide an experimental description of a complex three-dimensional flowfield and to give examples of its variation with changes in blowing rate, Mach number, and angle of attack. As computational fluid dynamics methods are developed to treat three-dimensional circulation-control flowfields, these data should serve as test cases for those methods.

Model

The model is a semispan wing incorporating circulation control by tangential blowing from a spanwise slot located ahead of a rounded trailing edge. The model was mounted on the sidewall of the tunnel on a turntable that could be manually rotated through a ± 5-deg range in angle of attack. The

wing-root mounting structure is covered by a fairing. Figure 1 is a sketch of the model installation in the tunnel showing the 0- and 45-deg sweep positions. The resulting aspect ratios are 4.0 and 1.85, respectively, based on the normal component of the exposed span. The sketch also shows the position of the boundary-layer traversing unit, which was mounted on a bracket attached to the tunnel centerbody support. Figure 2 shows the model in the 45-deg sweep position and the boundary-layer traversing unit.

The wing has a 20% elliptical section and a 25.4-cm constant chord, modified with circular leading and trailing edges of 4% radius (Fig. 3). This generic configuration does not represent a specific shape from current design concepts that are being developed. A full-span, tangential, rearward-blowing, circulation-control slot, with a nominal slot height of 0.0020 chord and a trailing-edge thickness of 0.0008 chord, was incorporated ahead of the trailing edge on the upper surface. Additional details of the wing design are given in Ref. 4.

Design suggestions based on experience with previous circulation-control tests were contributed by N. Wood, Stanford Institute for Aeronautics and Aeroacoustics, and by E. Rogers and J. Abramson, David W. Taylor Naval Ship Research and Development Center. Publications from their research are discussed in the review paper by Wood and Nielsen.[1] The model design closely follows the design concepts of Wood and Conlon.[5]

Instrumentation and Data Reduction

The pressure instrumentation consisted of 252 orifices on the wing, installed primarily at five spanwise stations along lines normal to the leading edge. A row of orifices was placed along a line at an angle of 45 deg with respect to the leading edge near midsemispan to assist in the analysis of the pressures at a sweep angle of 45 deg and to provide a row of orifices aligned with the location of the upper-surface boundary-layer measurements.

Three- and five-hole pitot/flow-direction probes were used to survey the wing boundary layer and wake. The probe tips used for most boundary-layer surveys are flattened three-hole probes, 0.15 mm in height; the three-hole probes were adjusted in pitch angle so that the tips were nearly parallel to the wing surface. The wake surveys were made with a five-hole probe having a tip diameter of 1.07 mm. In addition, some five-hole-probe surveys were made above the Coanda surface between the slot and the trailing edge. The tip of the five-hole probe was inclined upward 15 deg to reduce its flow interference in the wake downwash. The probes are similar to those described by Dudzinski and Krause.[6]

The traversing unit shown in Figs. 1 and 2 contains stepper motors that allow remote movement of the probe tip in the streamwise and vertical directions; the probe location is determined with the aid of encoders. A microcomputer-based probe control system allows manual operation of the unit and also provides an automatic mode in which data are obtained in a preprogrammed sequence of probe movements and data-acquisition cycles. The wing surface was located by electrical contact between the wing and the probe tip at the beginning of a boundary-layer survey.

Probe calibrations were performed in a free-jet calibration facility, following the procedures outlined by Dudzinski and

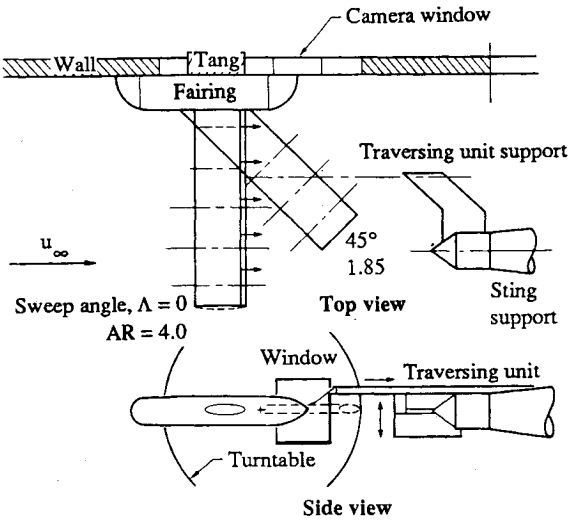

Fig. 1 Sketch of model and traversing unit installation.

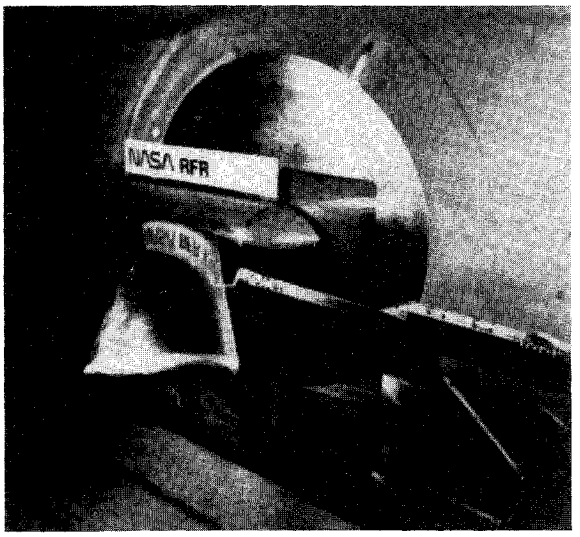

Fig. 2 Wing model at a sweep angle of 45 deg and probe traversing unit.

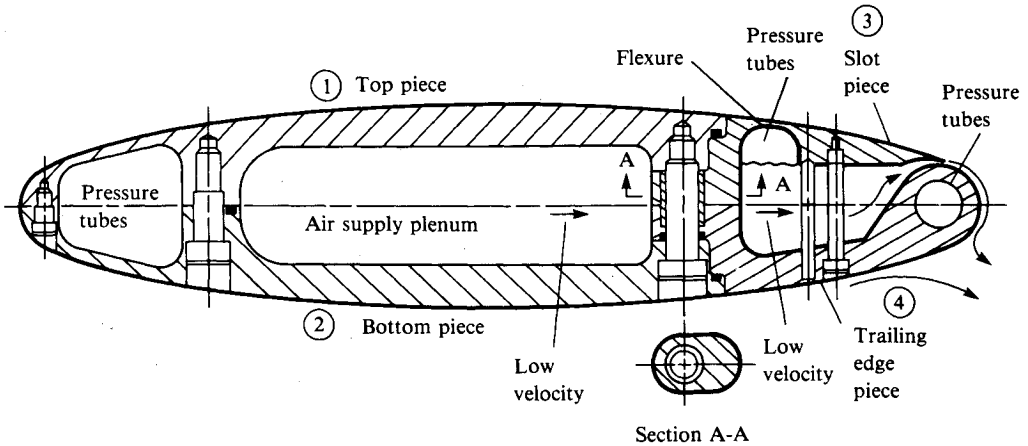

Fig. 3 Sketch of wing section showing four-piece construction, bolts, set screw, and adjusting screw for slot height.

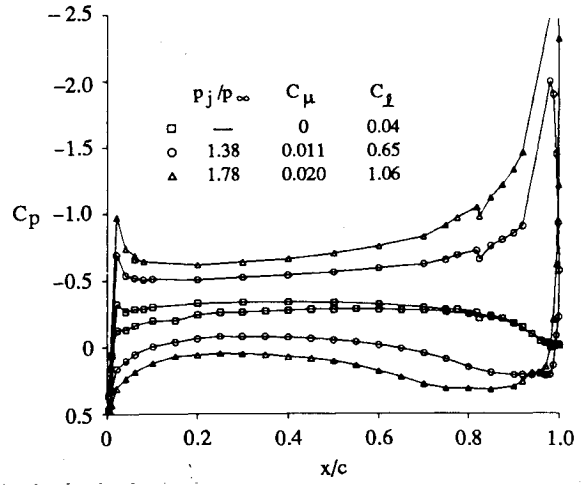

Fig. 4 Wing static-pressure distributions at midsemispan: M_∞ = 0.425; $Re_c = 2.27 \times 10^6$; $\alpha = 0$ deg.

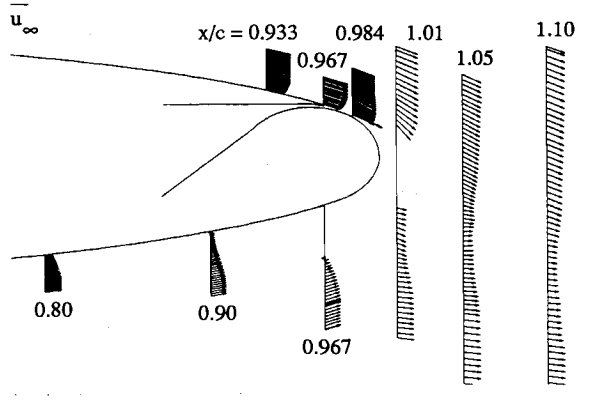

Fig. 5 Velocity components in streamwise section plane: M_∞ = 0.425; $\alpha = 0$ deg; $p_j/p_\infty = 1.4$.

Krause.[6] Calibrations were performed at six Mach numbers, ranging from 0.25 to 1.0. Three-hole-probe calibrations were performed over an angle range of ± 40 deg in the yaw plane; five-hole-probe calibrations were performed over a range of ± 40 deg in the pitch plane and +60 to −40 deg in the yaw plane, relative to the probe tip. Mach number and velocity profiles were computed from the three-hole-probe data with the aid of the local static pressure interpolated from the surface-orifice data. Pitot pressure, flow angles, and static pressure were determined from the five-hole-probe measurements. A search and interpolation procedure, in which the local Mach number was explicitly included as an independent variable, was performed on the entire probe-calibration data base.

The five-hole probe is too large to resolve the features of the flow near the Coanda surface with reasonable accuracy. Large excursions are present in the values of static pressure obtained from five-hole-probe measurements for $z/c < 0.0035$; these data have been discarded. The wall-jet data obtained with the three-hole probes were reduced using static-pressure distributions measured with the five-hole probe. These static-pressure distributions were plotted to an expanded scale and graphically extrapolated to the surface.

Test Conditions and Procedures

The wing pressures were first measured without boundary-layer trips at $M_\infty = 0.70$ at zero sweep. Next, boundary-layer trips were installed on the wing by use of sifted glass spherules at 9% chord. Sublimation flow-visualization tests were made at a Mach number of 0.70 to verify that the estimated trip size of 0.23-mm diam was adequate to cause transition. When the wing was swept to 45 deg, a sublimation test verified that the trips were also effective at this angle.

Flow surveys were obtained at a 45-deg sweep angle, freestream Mach numbers M_∞ of 0.425 and 0.70, Reynolds numbers based on streamwise chord Re_c of 2.3×10^6 and 3.2×10^6, and ratios of jet stagnation to freestream static pressure p_j/p_∞ of 1.0 to 2.2. Most flow surveys were obtained at an angle of attack α of 0 deg. The Mach numbers 0.425 and 0.70 correspond to the Mach numbers 0.30 and 0.50 at zero sweep, determined from simple sweep theory, $M_\infty/\cos 45$ deg. Performance data corresponding to both the swept and unswept conditions are presented by Keener et al.[4] Boundary-layer surveys were made at midsemispan, from 20% chord to near the trailing edge on both upper and lower surfaces. Wake surveys were obtained in a region 1-30% chord downstream of the trailing edge.

Oil-flow-visualization tests were made at both sweep angles at several Mach numbers to assist the analysis of the pressure and boundary-layer measurements.[4]

Results and Discussion

Data Obtained at 0-Deg Angle of Attack

Three static-pressure distributions corresponding to test conditions for which probe data were obtained are shown in Fig. 4. The upper-surface data were obtained from the diagonal row of orifices located at the spanwise survey station, and the lower-surface data were interpolated to that station from the adjacent chordwise orifices. Blowing rates are indicated both by p_j/p_∞ and by the momentum coefficient C_μ, the jet momentum flux normalized by the freestream dynamic pressure, and the wing area. The corresponding section lift coefficient c_l is also shown. Pressure distributions corresponding to the two values of blowing are characterized by weak suction peaks at the leading edge, near-zero pressure gradients at midchord, and large suction peaks on the upper surface downstream of the jet. The flow is locally supersonic in this region at the higher blowing rate; the minimum value of C_p is −4.75 (not shown).

Figure 5 is a composite view in the streamwise section plane of the aft portion of the model, including the slot inlet, and the surrounding flowfield. The intersection of the circular

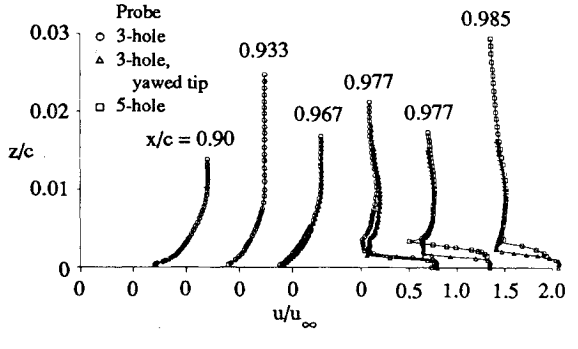

a) Velocity-magnitude profiles

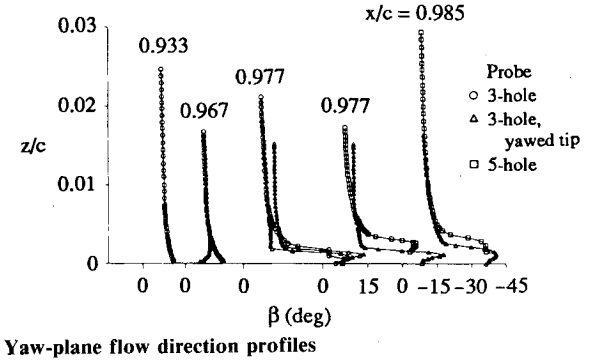

b) Yaw-plane flow direction profiles

Fig. 6 Upper-surface boundary-layer profiles: M_∞ = 0.425; $\alpha = 0$ deg; $p_j/p_\infty = 1.4$.

trailing-edge region of the model with this plane is an ellipse. The velocity vectors are projections in the streamwise plane, and the vector labeled u_∞ in the upper left corner corresponds to the freestream velocity. The boundary-layer profiles were obtained with a three-hole probe, and the vectors are drawn parallel to the local surface. The wake profiles and the flow survey at $x/c = 0.985$, above the Coanda surface downstream of the jet exit station, were obtained with a five-hole probe and are drawn at the measured inclination angle.

Figure 5 corresponds to $M_\infty = 0.425$, $\alpha = 0$ deg, and $p_j/p_\infty = 1.4$, the baseline test condition selected for flowfield surveys in this investigation. The boundary-layer profiles on the upper surface upstream of the slot and at the slot lip ($x/c = 0.967$) are full, showing the effect of entrainment by the jet. The jet is evident in the profile obtained at $x/c = 0.985$. A separated region is indicated by the lower-surface boundary-layer profiles. Significant variations in pitch-plane inclination angles are present in the wake profiles; the gradients decrease with increasing x/c. The gap in the wake profile at $x/c = 1.01$ is a region where the flow direction exceeded the probe calibration range. The upper portion of the wake nearest the trailing edge is characterized by large negative values of the pitch-plane angle. Below the trailing edge, the pitch-plane angles are still negative, but are smaller in magnitude. Large cross-stream velocity components are present in this flowfield; the cross-stream flow is shown in subsequent figures.

Figure 6 presents conventional velocity-magnitude and flow-angularity profiles for the trailing-edge, upper-surface locations surveyed at the baseline test condition of Fig. 5. Velocity magnitudes are normalized by the freestream velocity and plotted against z/c, the distance from the surface normalized by the streamwise chord. The distance from the surface z is measured normal to the tunnel axis, which is also normal to

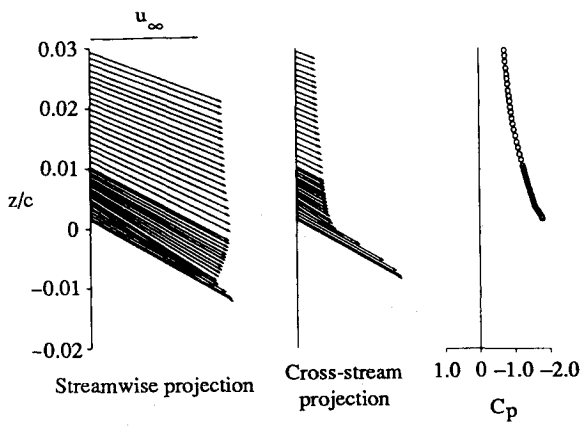

Fig. 7 Velocity and static-pressure profiles above the Coanda surface: $M_\infty = 0.425$; $\alpha = 0$ deg; $p_j/p_\infty = 1.4$; $x/c = 0.984$.

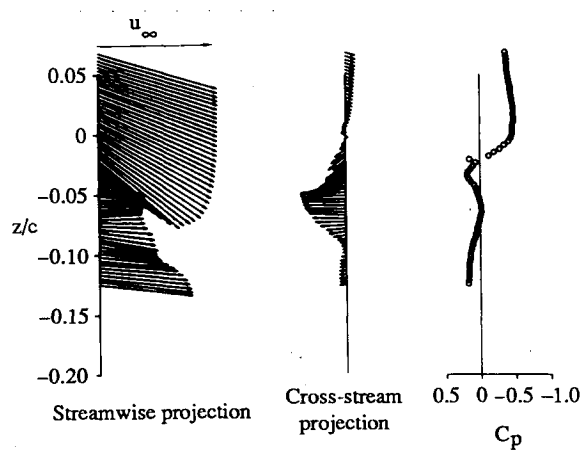

Fig. 8 Wake velocity and static-pressure profiles: $M_\infty = 0.425$; $\alpha = 0$ deg; $p_j/p_\infty = 1.4$; $x/c = 1.02$.

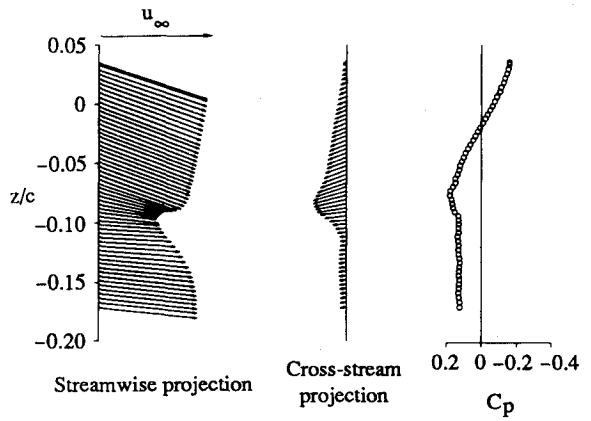

Fig. 9 Wake velocity and static-pressure profiles: $M_\infty = 0.425$; $\alpha = 0$ deg; $p_j/p_\infty = 1.4$; $x/c = 1.10$.

the mean plane of the wing at $\alpha = 0$ deg. The yaw-plane flow angle β is defined to be positive for outboard flow. The profiles of β upstream of the slot indicate that the flow was approximately colinear, with a mean inboard inclination that increases with increasing downstream distance. Both the thin, full character of the velocity-magnitude profiles near the slot station and the inboard values of β imply strong entrainment by the jet. Profiles obtained with both the straight and yawed three-hole probes and the five-hole probe are shown for $x/c = 0.977$ and 0.985. Agreement among the profiles at $x/c = 0.977$ with the three-hole probes is good for both u/u_∞ and β; agreement is also good between the three- and five-hole probe data at $x/c = 0.977$ and 0.985 in the region above the jet. The two wall-jet profiles show that the jet is directed normal to the slot ($\beta \approx -45$ deg).

Close-ups of profiles corresponding to the baseline test condition are presented in Figs. 7–9. These data were obtained with the five-hole probe and are presented in the form of streamwise velocity components, cross-stream velocity components (velocity components lying in a plane normal to the freestream velocity vector), and static-pressure distributions. The profiles of Figs. 7–9 correspond to $x/c = 0.984$, 1.02, and 1.10, respectively. The streamwise profiles at $x/c = 0.984$ and 1.10 are also shown in Fig. 5. The velocity vectors are plotted to the same scale in Figs. 7–9, but differences in static pressure among the profiles required significant changes in the C_p scale.

In reducing the data shown in Fig. 7 corresponding to $0 \le z/c \le 0.0035$, the static pressure was extrapolated from the region above the jet to the surface, the stagnation pressure was assumed to be the maximum of the values measured by the probe orifices, and the pitch-plane flow direction was assumed to be parallel to the local surface.

The contrast between the inboard inclination of the entire profile at $x/c = 0.984$ and the outboard flow in the centers of the wake profiles is evident in these figures, as are the substantial variations in static pressure. As expected, the gradients decrease with increasing distance downstream.

The origin of the z coordinate for the wake profiles is the upper lip of the slot. The upper edge of the wake near the trailing edge is characterized by high velocity magnitudes, large downwash, and nearly streamwise flow in the yaw plane; the lower edge has lower velocity magnitudes and is more nearly streamwise in both planes. The flow in the central portion of the wake is predominantly outboard, despite the fact that the jet, which is strong enough to control the wing circulation, is directed 45 deg inboard. At $x/c = 1.02$, the flow at the center of the wake is approximately parallel to the trailing edge. Apparently, the flow in the viscous central wake is dominated by the outboard flow in the separated region on the lower surface.

The view of the flowfield structure deduced from probe data is reinforced by oil-flow-visualization data. Oil-flow pho-

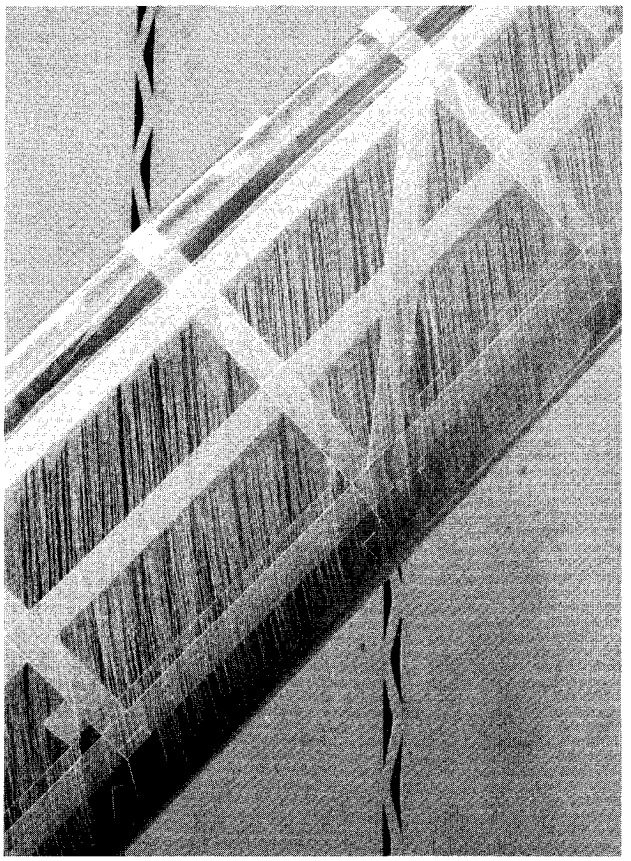

a) Central portion of upper surface

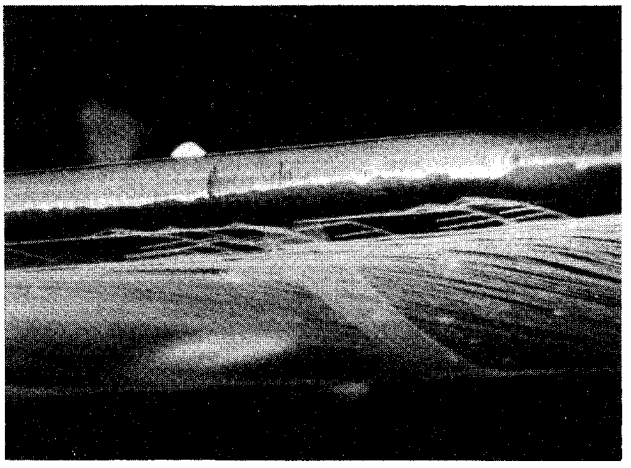

b) Central portion of trailing-edge region, viewed from below

Fig. 10 Oil-flow-visualization photographs: $M_\infty = 0.425$; $\alpha = 0$ deg; $p_j/p_\infty = 1.4$.

tographs obtained at the baseline test condition are shown in Fig. 10. Figure 10a shows the central region of the upper surface, and Fig. 10b shows the center of the trailing-edge region, viewed from below. Prior to the run, a single spanwise strip of oil was applied to each surface downstream of the boundary-layer trip. During the run, the oil flowed rearward in streaks, forming the flow pattern. At the slot, it was found that sufficient oil was ejected onto the Coanda surface to form a flow pattern.

The upper-surface oil pattern shows primarily streamwise flow, with slight inboard turning upstream of the slot. The lower-surface oil pattern (Fig. 10b) is a typical swept-wing separation pattern, in which the surface flow direction becomes more nearly parallel to the trailing edge with increasing downstream distance until a well-defined limiting line is reached. The flow exterior to the lower-surface boundary layer is more nearly streamwise, so that the boundary-layer flow is highly three dimensional. The flow direction indicated by several oil streaks within the separated region (the dark strip in the center of Fig. 10b) is outboard along the wing, parallel to the separation line. It is surprising that the oil pattern on the Coanda surface (Fig. 10b) shows flow normal to the slot until it reaches the equally well-defined upper-surface separation line, with no indication of outboard flow. The result is a dramatic contrast between the upper- and lower-surface separation lines, in which flow at the lower-surface separation line is parallel to the trailing edge and the flow leaves the upper-surface separation line normal to the trailing edge. There is large skewing within the boundary layers coming off

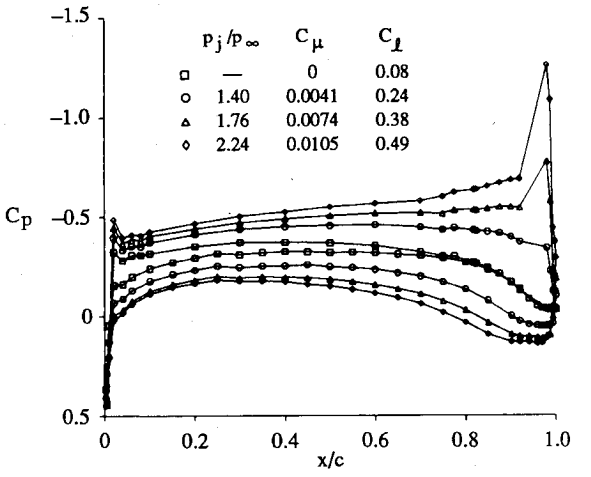

Fig. 11 Wing static-pressure distributions at midsemispan: $M_\infty = 0.70$; $Re_c = 3.15 \times 10^6$; $\alpha = 0$ deg.

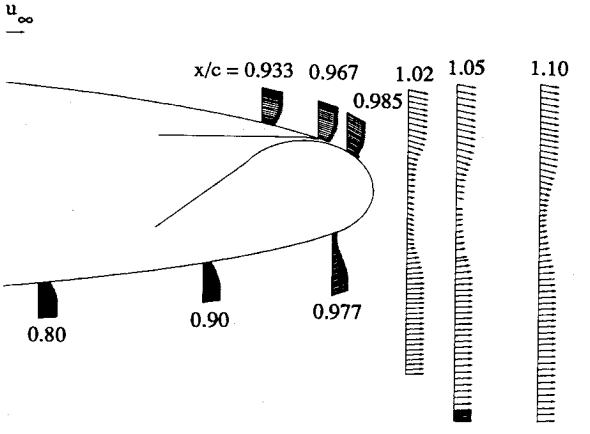

Fig. 12 Velocity components in streamwise section plane: $M_\infty = 0.70$; $\alpha = 0$ deg; $p_j/p_\infty = 1.4$.

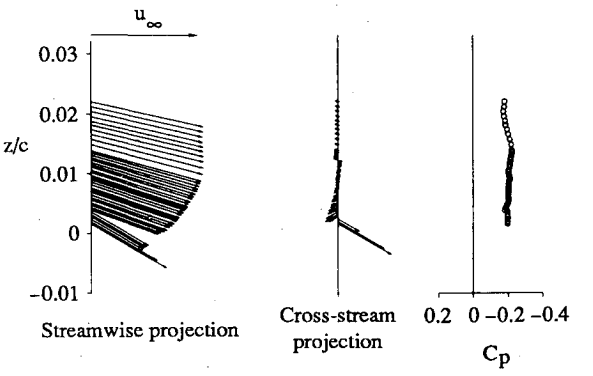

Fig. 13 Velocity and static-pressure profiles above the Coanda surface: $M_\infty = 0.700$; $\alpha = 0$ deg; $p_j/p_\infty = 1.4$; $x/c = 0.985$.

both the upper and lower surfaces. Computations of this highly three-dimensional flowfield will be especially interesting.

Static-pressure distributions corresponding to no blowing and three blowing rates at $M_\infty = 0.70$ and $\alpha = 0$ deg, including test conditions for which boundary-layer and wake data were obtained, are presented in Fig. 11. The data correspond to approximately the same pressure-ratio range as those of Fig. 4, but the values of C_μ and c_l are smaller.

The composite view presented in Fig. 12, and the detailed profile data of Figs. 13–15, correspond to $M_\infty = 0.70$, the same jet pressure ratio as in Fig. 5, $p_j/p_\infty = 1.4$, but a lower jet momentum coefficient, $C_\mu = 0.0041$. The influence of the jet on the surrounding flow is clearly much less pronounced at this test condition. The upper-surface boundary-layer profiles in the vicinity of the jet are less full and show positive values of β near the surface upstream of the jet and at the location of minimum velocity in the profile downstream of the jet. The lower-surface separation line is apparently near the last measuring station on the lower surface. The reduced circulation is indicated by the reduced downward displacement of the wake centerline, relative to the data of Fig. 5.

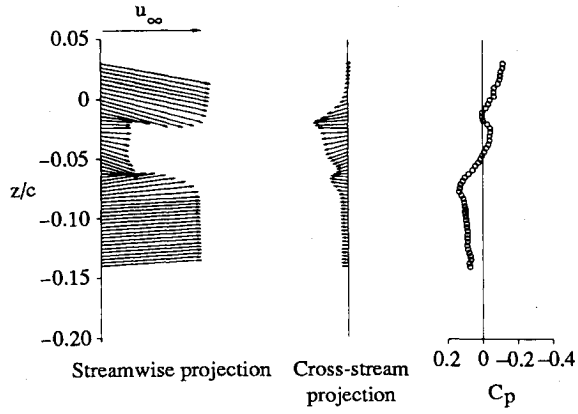

Fig. 14 Wake velocity and static-pressure profiles: $M_\infty = 0.700$; $\alpha = 0$ deg; $p_j/p_\infty = 1.4$; $x/c = 1.02$.

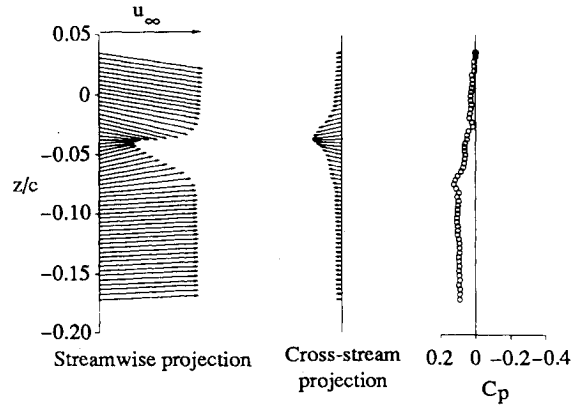

Fig. 15 Wake velocity and static-pressure profiles: $M_\infty = 0.700$; $\alpha = 0$ deg; $p_j/p_\infty = 1.4$; $x/c = 1.1$.

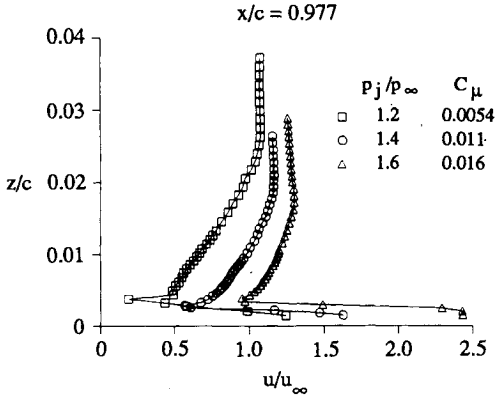

Fig. 16 Velocity-magnitude profiles: $M_\infty = 0.425$; $\alpha = 5$ deg.

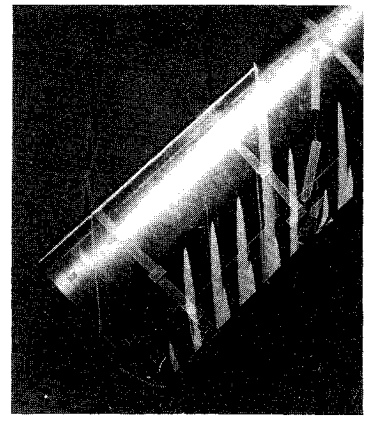

a)

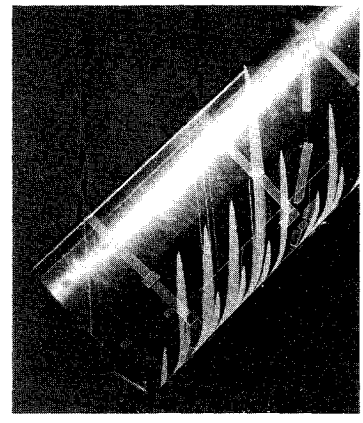

b)

Fig. 17 Fluorescent oil-flow photographs of wing upper surface: $M_\infty = 0.425$; $\alpha = 5$ deg.

Data Obtained at 5-Deg Angle of Attack

The next group of figures illustrates an abrupt transition from incipient separation at the slot location to attached flow at $M_\infty = 0.425$ and $\alpha = 5$ deg. Velocity-magnitude profiles downstream of the jet exit location, $x/c = 0.977$, are shown in Fig. 16 for three blowing rates. The shape of the velocity profile above the jet corresponding to $p_j/p_\infty = 1.2$ is characteristic of a boundary layer near separation, and the minimum value of velocity measured at the interface between the wall jet and the outer flow is low, indicating minimal entrainment of the outer flow by the jet. The situation for $p_j/p_\infty = 1.4$ is different, in that the boundary-layer portion of the profile is relatively thin and full and the minimum value of velocity is significantly greater. The velocity magnitudes are higher at the next higher blowing rate, $p_j/p_\infty = 1.6$, but the qualitative features are similar to those exhibited by the profile corresponding to $p_j/p_\infty = 1.4$.

Figure 17 shows two upper surface fluorescent oil-flow photographs corresponding to $M_\infty = 0.425$, $\alpha = 5$ deg, and $p_j/p_\infty = 1.2$ and 1.3, obtained from Keener et al.[4] The oil was injected from surface orifices and photographed during a run. At the lower blowing rate, the oil streaks turn toward the spanwise direction near the slot, indicating separation at the slot, except in the immediate vicinity of the tip. The pattern obtained for $p_j/p_\infty = 1.3$ is significantly different, showing streamwise flow along the span up to the slot, indicating attached flow at the slot.

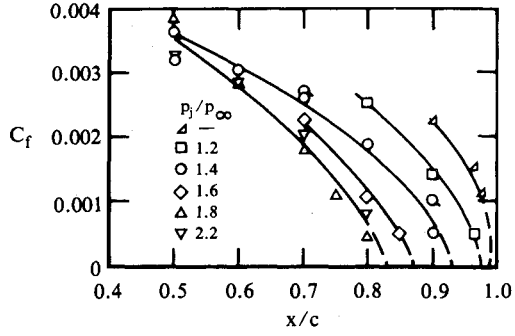

Fig. 18 Lower-surface skin-friction distributions: $M_\infty = 0.425$; $\alpha = 0$ deg.

Evidence of similar behavior was not observed at $M_\infty = 0.70$ and $\alpha = 5$ deg. The jet flow was much less effective in maintaining attached flow at the slot at this Mach number.

Lower-Surface Skin-Friction Distributions

Values of skin-friction coefficient C_f were determined from the attached boundary-layer profiles by fitting the inner region of the velocity magnitude profiles to the following generally accepted similarity law,

$$\frac{u}{u_\tau} = \frac{1}{0.41} \ln\left(\frac{zu}{\nu}\right) + 5.0 \qquad (1)$$

Application of this method to skewed boundary layers is discussed in Ref. 7.

The influence of blowing rate on the position of the lower-surface separation line is shown in Fig. 18, in which C_f is plotted as a function of x/c for a range of blowing rates. It is assumed that extrapolation of values of C_f to zero provides a reasonable estimate of the separation-line location. (Actually, the velocity magnitudes become small and the local flow direction becomes parallel to the wing trailing edge near separation.) It is shown that the separation line moves upstream with increasing blowing rate, up to $p_j/p_\infty = 1.8$, but an additional increase of p_j/p_∞ to 2.2 does not produce an additional forward movement of the separation line. It is in this range of blowing rates that the performance data (c_l vs C_μ) show no additional increase of lift with increasing blowing rate.

Concluding Remarks

Boundary-layer and wake-survey data were obtained at midsemispan in the flow about a 45-deg swept, circulation-control wing at freestream Mach numbers of 0.425 and 0.70. Boundary-layer profiles forward on the wing on both upper and lower surfaces are approximately streamwise and two dimensional. The flow in the vicinity of the jet exit and in the near wake is highly three dimensional. Qualitative variations in flowfield features with freestream Mach number and jet blowing rate are illustrated by velocity vector plots. The jet flow near the slot on the Coanda surface is directed normal to the slot, or 45 deg inboard. All near-wake surveys, including surveys obtained 1% chord downstream of the trailing edge, show large outboard flows at the center of the wake. At Mach 0.425 and 5-deg angle of attack, a range of jet blowing rates was found for which an abrupt transition from incipient separation to attached flow occurs in the boundary layer upstream of the slot. The variation in the lower-surface separation location with blowing rate was determined from boundary-layer measurements at Mach 0.425.

Acknowledgments

This research was conducted under the McDonnell Douglas Independent Research and Development Program in cooperation with NASA Ames Research Center.

References

[1]Wood, N. J., and Nielsen, J. N., "Circulation Control Airfoils Past, Present, Future," AIAA Paper 85-0204, Jan. 1985.

[2]Spaid, F. W., and Keener, E. R., "Boundary-Layer and Wake Measurements on a Swept, Circulation-Control Wing," NASA CP-2432, Aug. 1986.

[3]Spaid, F. W., and Keener, E. R., "Boundary-Layer and Wake Measurements on a Swept, Circulation-Control Wing," NASA TM 89426, Dec. 1987.

[4]Keener, E. R., Sanderfer, D. T., and Wood, N. J., "Pressure Distributions and Oil-Flow Patterns for a Swept Circulation-Control Wing," NASA CP-2432, Aug. 1986.

[5]Wood, N. J., and Conlon, J. A., "The Performance of a Circulation Control Airfoil at Transonic Speeds," AIAA Paper 83-0083, Jan. 1983.

[6]Dudzinski, T. J., and Krause, L. N., "Flow-Direction Measurement with Fixed-Position Probes," NASA TM X-1904, Oct. 1969.

[7]Spaid, F. W., "Transonic Airfoil and Wing Flowfield Measurements," AIAA Paper 84-0100, Jan. 1984.